

Prospects of measuring the CKM matrix element $|V_{ts}|$ at the LHC

Ahmed Ali*

*Deutsches Elektronen-Synchrotron DESY, D-22607 Hamburg, Germany*Fernando Barreiro[†] and Theodota Lagouri[‡]*Universidad Autonoma de Madrid (UAM), Facultad de Ciencias C-XI,**Departamento de Fisica, Cantoblanco, Madrid 28049, SPAIN***Abstract**

We study the prospects of measuring the CKM matrix element $|V_{ts}|$ at the LHC with the top quarks produced in the processes $pp \rightarrow t\bar{t}X$ and $pp \rightarrow t/\bar{t}X$, and the subsequent decays $t \rightarrow W^+s$ and $\bar{t} \rightarrow W^-\bar{s}$. To reduce the jet activity in top quark decays, we insist on tagging the W^\pm leptonically, $W^\pm \rightarrow \ell^\pm\nu_\ell$ ($\ell = e, \mu, \tau$), and analyse the anticipated jet profiles in the signal process $t \rightarrow Ws$ and the dominant background from the decay $t \rightarrow Wb$. To that end, we analyse the V_0 (K^0 and Λ) distributions in the s - and b -quark jets concentrating on the energy and transverse momentum distributions of these particles. The V_0 s emanating from the $t \rightarrow Wb$ branch have displaced decay vertexes from the interaction point due to the weak decays $b \rightarrow c \rightarrow s$ and the b -quark jets are rich in charged leptons. Hence, the absence of secondary vertexes and of the energetic charged leptons in the jet provide additional (b -jet vs. s -jet) discrimination in top quark decays. These distributions are used to train a boosted decision tree (BDT), a technique used successfully in measuring the CKM matrix element $|V_{tb}|$ in single top production at the Tevatron. Using the BDT classifier, and a variant of it called BDTD, which makes use of decorrelated variables, we calculate the BDT(D)-response functions corresponding to the signal ($t \rightarrow Ws$) and background ($t \rightarrow Wb$). Detailed simulations undertaken by us with the Monte Carlo generator PYTHIA are used to estimate the background rejection versus signal efficiency for three representative LHC energies $\sqrt{s} = 7$ TeV, 10 TeV and 14 TeV, of which only the analysis for the $\sqrt{s} = 14$ TeV case is shown in detail. We argue that a benchmark with 10% accuracy for the signal ($t \rightarrow Ws$) at a background ($t \rightarrow Wb$) rejection by a factor 10^3 (required due to the anticipated value of the ratio $|V_{ts}|^2/|V_{tb}|^2 \simeq 1.6 \times 10^{-3}$) can be achieved at the LHC@14 TeV with an integrated luminosity of 10 fb^{-1} .

PACS numbers:

*Electronic address: ahmed.ali@desy.de

†Electronic address: fernando.barreiro@uam.es

‡Electronic address: theodota.lagouri@cern.ch

I. INTRODUCTION

It is now fifteen years that the top quark was discovered in proton-antiproton collisions at the Tevatron [1, 2]. Since then, a lot of precise measurements have been undertaken at the two Fermilab experiments, CDF and D0. Among the highlights are the measurements of the top quark mass, currently having an accuracy of about 0.75%, the $t\bar{t}$ production cross section with about 9% accuracy [3], and the observation of the electroweak single top production [4, 5]. Of these, the single top (or anti-top) production cross section depends on the charged current couplings tqW , where $q = d, s, b$, which in the standard model (SM) are governed by the Cabibbo-Kobayashi-Maskawa (CKM) quark mixing matrix V_{CKM} [6, 7]:

$$V_{\text{CKM}} \equiv \begin{pmatrix} V_{ud} & V_{us} & V_{ub} \\ V_{cd} & V_{cs} & V_{cb} \\ V_{td} & V_{ts} & V_{tb} \end{pmatrix} .$$

In the Wolfenstein Parametrisation [8], this matrix is expressed as

$$V_{\text{CKM}} \simeq \begin{pmatrix} 1 - \frac{1}{2}\lambda^2 & \lambda & A\lambda^3(\rho - i\eta) \\ -\lambda(1 + iA^2\lambda^4\eta) & 1 - \frac{1}{2}\lambda^2 & A\lambda^2 \\ A\lambda^3(1 - \rho - i\eta) & -A\lambda^2(1 + i\lambda^2\eta) & 1 \end{pmatrix} ,$$

where A , λ , ρ and η are the Wolfenstein parameters.

The cross section $\sigma(p\bar{p} \rightarrow t/\bar{t}X)$ has provided the first direct measurement of the dominant CKM-matrix element $|V_{tb}|$. In this analysis, it is assumed that the CKM matrix elements $|V_{td}|$ and $|V_{ts}|$ are much smaller than $|V_{tb}|$, but no assumption is made about the unitarity of the 3×3 CKM matrix. To obtain $|V_{tb}|^2$, the measured cross section for an summed top quark mass is divided by the theoretical cross section for $|V_{tb}| = 1$. Following this procedure, the CDF measurements yield $|V_{tb}| = 0.91 \pm 0.11(\text{stat} + \text{syst}) \pm 0.07(\text{theory})$, which in turn gives $|V_{tb}| > 0.71$ at 95% C.L. [5]. The corresponding limit from D0 is $|V_{tb}| > 0.78$ at 95% C.L. [4]. The combined CDF and D0 analysis assumes 170 GeV as the top quark mass and yields $|V_{tb}| = 0.91 \pm 0.08$ with $|V_{tb}| > 0.79$ at 95% C.L. using $\sigma(p\bar{p} \rightarrow t/\bar{t} + X) = 3.14$ pb [10]. A theoretical value $\sigma(p\bar{p} \rightarrow t/\bar{t} + X) = 3.46$ pb [9] as input yields $|V_{tb}| = 0.88 \pm 0.07$ with $|V_{tb}| > 0.77$ at 95% C.L. [11]. There also exist limits on this matrix element obtained from the decays of the top quarks by tagging the b-quark jet in the final state. Defining the ratio $R_{t\text{equiv}} \frac{\mathcal{B}(t \rightarrow bW)}{\mathcal{B}(t \rightarrow dW) + \mathcal{B}(t \rightarrow sW) + \mathcal{B}(t \rightarrow bW)} = |V_{tb}|^2$, where use has been made of the CKM unitarity in the second equality, CDF and D0 measurements yield $|V_{tb}| > 0.78$ [12] and $|V_{tb}| > 0.89$ [13], respectively.

The above determination of the matrix element $|V_{tb}|$, obtained from the direct single top production and the b -tagged decays of the top quark, can be compared with the indirect determination of the same based on a number of loop-induced processes in which top quark participates as a virtual

state, such as the B^0 - \overline{B}^0 and B_s^0 - \overline{B}_s^0 mixings, the radiative decay $B \rightarrow X_s \gamma$ and the CP-violation parameter ϵ_K in the Kaon sector. Overall fits of the CKM unitarity yield, comparatively speaking, an infinitely more accurate value $|V_{tb}| = 0.999133(44)$ [14]. This precision, in all likelihood, will not be matched by the *direct determination* of $|V_{tb}|$, as experiments at the LHC are expected to reach an accuracy of a few per cent on this quantity. Nevertheless, a determination of $|V_{tb}|$ with such an accuracy will be very valuable to constrain beyond-the-SM physics models. A good case in point is a model with four generations, in which $|V_{tb}|$ can be as low as 0.93 [15].

We go a step further and explore in this paper the prospects of measuring the matrix element $|V_{ts}|$ at the LHC. In the Wolfenstein parametrisation [8], this matrix element is given as $|V_{ts}| = A\lambda^2 + O(\lambda^4)$. The best-fit values from the unitarity fits are: $A = 0.814$, $\lambda = 0.2257$, yielding $|V_{ts}| = 0.0407 \pm 0.001$ [14]. The smallest matrix element in the third row of the CKM matrix is V_{td} , and its value from the CKM unitarity fit is posted as $|V_{td}| = A\lambda^3 \sqrt{(1-\rho)^2 + \eta^2} = (8.74_{-0.37}^{+0.26}) \times 10^{-3}$. Direct determination of these matrix elements will require a good tagging of the $t \rightarrow s$ transition (for $|V_{ts}|$) and $t \rightarrow d$ transition (for $|V_{td}|$) in the top quark decays, and a very large top quark statistics, which will be available only at the LHC in the foreseeable future from the processes $pp \rightarrow t\bar{t} + X$ and $pp \rightarrow t/\bar{t} + X$. Just as for the direct measurement of $|V_{tb}|$, there is also a lot of interest in the direct measurements of V_{ts} and V_{td} , as the absolute values of these CKM matrix elements can be modified by approximately a factor 2 from their SM values quoted above, taking the example of a four-generation extension of the SM [15]. Lacking a good tagging for the $t \rightarrow d$ transition, and also because of the small size of the CKM-matrix element, $|V_{td}| = O(10^{-2})$, we concentrate here on the direct measurements of $|V_{ts}|$ at the LHC.

In order to be able to measure $|V_{ts}|$ directly, one has to develop efficient discriminants to suppress the dominant decay $t \rightarrow W b$. As the first step, we propose to tag only those events in which the W^\pm decay leptonically to reduce the jet activity in top quark decays. The emerging s -quark from the top quark decay $t \rightarrow W s$, and the collinear gluons which are present in the fragmentation process anyway, will form a hadron jet. We suggest tagging on the V_0 s (K^0 s and Λ s) in this jet, and measure their energy and transverse momentum distributions. Energetic V_0 s are also present in the b -quark jets initiated by the decay $t \rightarrow W b$ and the subsequent weak decays $b \rightarrow c \rightarrow s$. However, in this case, the V_0 s will be softer, will have displaced vertexes (from the interaction point) and they will be often accompanied with energetic charged leptons due to the decays $b \rightarrow \ell^\pm X$. Absence of a secondary vertex and paucity of the energetic charged leptons in the jet provide a strong discrimination on the decays $t \rightarrow W b$ without essentially compromising the decays $t \rightarrow W s$. Thus, the scaled energy and transverse momentum distributions of the K^0 s, Λ s and ℓ^\pm s, and the secondary decay vertex distributions (dN/dr) are the quantities of principal interest. Here r is the distance traversed in the transverse plane, i.e. the plane perpendicular to

the beam axis or $r - \phi$ plane, by the b -quark before decaying, smeared with a Gaussian resolution to take into account realistic experimental conditions.

We have assumed two representative r.m.s. values ($\sigma(\text{vertex}) = 1 \text{ mm}$ and 2 mm) for the Gaussian, where 2 mm is more realistic. Experimentally, b -tagging algorithms are based on measurements of the impact parameter from the B meson charged tracks. The power separation between b - and light-jets using this so called 2D-method is similar to the one we used in our analysis with 2 mm resolution. We also show results with 1 mm resolution in order to illustrate how important it will be for the Super LHC (SLHC) to improve on the b -tagging efficiency. These distributions are calculated for the processes $pp \rightarrow t\bar{t}X$ and $pp \rightarrow t/\bar{t}X$, for the signal ($t \rightarrow W s$) and background ($t \rightarrow W b$).

Having generated these distributions, characterising the signal $t \rightarrow W s$ and the background $t \rightarrow W b$ events, we use a technique called the Boosted Decision Tree (BDT) – a classification model used widely in data mining [16] – to develop an identifier optimised for the $t \rightarrow W s$ decays. In our calculation, we use both BDT and a variant of it called BDTD (here D stands for decorrelated), where possible correlations in the input variables are removed by a proper rotation obtained from the decomposition of the square root of the covariance matrix, to discriminate the signal events from the large backgrounds. We recall that this technique has been successfully used to establish the single top quark production in $p\bar{p}$ collisions at the Tevatron [4, 5] (see [17] for details). Briefly, the generated input is used for the purpose of training and testing the samples. We provide the input in terms of the variables discussed earlier for the signal ($t \rightarrow W s$) and the background ($t \rightarrow W b$), obtained with the help of a Monte Carlo generator. This information is used to develop the splitting criteria to determine the best partitions of the data into signal and background to build up a decision tree (DT). The separation algorithm used in splitting the group of events in building up DT plays an important role in the performance. The software called the Toolkit for Multivariate Data Analysis in ROOT (TMVA) [18] is used for the BDT(D) responses in our analysis. Detailed simulations presented here are done using PYTHIA [19] to model the production processes, gluon radiation, fragmentation and decay chains, and the underlying events. We calculate the signal ($t \rightarrow W s$) efficiencies for two cases called bb/b_s and bs/ss (defined in section II) for an assumed (Gaussian) vertex smearing with an r.m.s. value of 2mm and 1mm . Concentrating on the bb/b_s case, when only one of the top (or antitop) quark decays via $t \rightarrow sW^+$, compared to the case when both the top and antitop decay via the dominant transition $t \rightarrow bW^+$, these efficiencies lie typically between 5% (for the 2mm smearing) and 20% (for the 1mm case) for a background ($t \rightarrow W b$) rejection by a factor 10^3 (see Table I).

Note that this level of background rejection is necessary due to the anticipated value of the ratio $|V_{ts}|^2/|V_{tb}|^2 \simeq 1.6 \times 10^{-3}$. The required integrated LHC luminosity to determine $|V_{ts}|$ *directly*

is estimated as 10 fb^{-1} at 14 TeV. Numerical analysis reported here is carried out for three representative LHC energies: $\sqrt{s} = 7 \text{ TeV}$, 10 TeV and 14 TeV , but we present the detailed results only for $\sqrt{s} = 14 \text{ TeV}$ as the distributions for $\sqrt{s} = 7 \text{ TeV}$ and 10 TeV are similar to the 14 TeV case.

In section 2, we study the process $pp \rightarrow t\bar{t}X$, reviewing first the production cross sections at the LHC energies. The energy-momentum profiles of the signal ($t \rightarrow W s$) and background ($t \rightarrow Wb$) events produced in the $t\bar{t}$ pair production process and the subsequent decays $pp \rightarrow t(\rightarrow W^+b) \bar{t}(\rightarrow W^- \bar{b})X$, $pp \rightarrow t(\rightarrow W^+b) \bar{t}(\rightarrow W^- \bar{s})X$, $pp \rightarrow t(\rightarrow W^+s) \bar{t}(\rightarrow W^- \bar{b})X$ and $pp \rightarrow t(\rightarrow W^+s) \bar{t}(\rightarrow W^- \bar{s})X$ are worked out. The last of these has a very small branching ratio and its measurement would require a huge LHC luminosity (we included this case for the sake of completeness). Tagging efficiencies for $pp \rightarrow t\bar{t}X$ calculated with the BDT(D) classifier are shown in Table 1. Numerical results in this table are presented as (bb/bs) and (bs/ss) , corresponding to the cases when only one of the t (or \bar{t}) decays via $t \rightarrow W^+ s$ (or $\bar{t} \rightarrow W^- \bar{s}$) and when both the t and \bar{t} decay via $t \rightarrow W^+ s$ and $\bar{t} \rightarrow W^- \bar{s}$, respectively.

Section 3 is a repeat of the above analysis for the single top production process $pp \rightarrow t/\bar{t}X$ at the LHC. The end-product of this analysis chain is again the background rejection vs. the signal efficiency based on the BDT(D) response functions. The tagging efficiencies, calculated for $\sqrt{s} = 7, 10, \text{ and } 14\text{TeV}$ with the BDTD classifier are presented in Table 2. Section 4 briefly summarises our results and outlook.

II. ANALYSIS OF THE PROCESS $pp \rightarrow t\bar{t}X$ AND THE SUBSEQUENT DECAYS $t \rightarrow Wb, Ws$

Theoretical predictions of the top quark production at the LHC have been obtained by including up to the next-to-next-to-leading order (NNLO) corrections in the strong coupling constant [22–25]. They have been updated taking into account modern parton distribution functions (PDFs) [26, 27]. A typical estimate is: $\sigma(pp \rightarrow t\bar{t}X) = 874_{-33}^{+14} \text{pb}$ for $m_t = 173 \text{ GeV}$ and $\sqrt{s} = 14 \text{ TeV}$ [28], where the errors reflect the combined uncertainties in the factorisation and normalisation scales and in the parton distribution functions (PDF). Other independent NNLO calculations yield similar cross section, though the error budgeting is somewhat different. Kidonakis and Vogt [24] put the cross section $\sigma(pp \rightarrow t\bar{t}X) = 894 \pm 4(\text{kinematics})_{-44}^{+68}(\text{scale})_{-31}^{+29}(\text{PDF})$ for the same values of m_t and \sqrt{s} , using the CTEQ6.6M PDFs [27], and $\sigma(pp \rightarrow t\bar{t}X) = 943 \pm 4(\text{kinematics})_{-49}^{+77}(\text{scale}) \pm 12(\text{PDF})$, using the MRST 2006 PDFs [26]. Compared to the $t\bar{t}$ production cross section at the Tevatron ($\sqrt{s} = 1.96 \text{ TeV}$), $\sigma(p\bar{p} \rightarrow t\bar{t}X) = 7.34_{-0.38}^{+0.23} \text{ pb}$ [28], one expects a rise in the $t\bar{t}$ cross section by more than two orders of magnitude between the Tevatron and the LHC@14 TeV. The cross sections at the lower LHC energies, 7 and 10 TeV, have also been calculated [24, 28], with $\sigma(pp \rightarrow t\bar{t}X) \simeq 400$

pb at 10 TeV and about half that number at 7 TeV. Thus, for the top quark physics, the dividends in going from 7 to 14 TeV are higher by a good factor 4.

For the numerical results shown here we have used the PYTHIA Monte Carlo [19] to generate 10^6 events for the process $pp \rightarrow t\bar{t}X$, followed by the decay chains $t \rightarrow W^+b$, W^+s and $\bar{t} \rightarrow W^-\bar{b}$, $W^-\bar{s}$. As stated in the introduction, the W^\pm are forced to decay only leptonically $W^\pm \rightarrow \ell^\pm\nu_\ell$ ($\ell = e, \mu, \tau$) to reduce the jet activity from the non-leptonic decays of the W^\pm . This corresponds to an integrated luminosity of 10 fb^{-1} at 14 TeV. For an estimated efficiency of 5% at a 10^{-3} background rejection, and $|V_{ts}|^2 \simeq 1.7 \times 10^{-3}$, as in the SM, this means that we expect $0.05 \times 2 \times 1.7 \times 10^{-3} \times 10^6 = 170$ signal events with a background of $10^{-3} \times 10^6 = 10^3$ events, giving a significance of $170/\sqrt{1000}$ i.e. more than 5σ .

We then concentrate on the $V0$ production, which for the experimental conditions at the two main detectors ATLAS [20] and the CMS [21] implies $V0 = K_S^0$ or $V0 = \Lambda$, as the long-lived K_L^0 will decay mostly out of the detectors. However, both K_S^0 and Λ can be detected by ATLAS and CMS and their energy and momentum measured with reasonably good precision. In the present analysis, we reconstruct $V0$ s and soft leptons in the rapidity range $|\eta| \leq 2.5$ [20]. In addition, we require the $V0$'s decay radius to lie in the range 20 to 600 mm. These acceptance cuts are acceptable for both multipurpose detectors mentioned above, and they will be used in the analysis described in this and the next section.

We will show the distributions for $\sqrt{s} = 14 \text{ TeV}$, the designed LHC center-of-mass energy. The K^0 -energy distribution is shown in the left-hand frame in Fig 1 plotted as a function of the scaled energy $X_K = E_K/E_{\text{jet}}$. For this study, the jet energy is set equal to the quark energy produced in the decay $t \rightarrow Wb, Ws$. In a realistic simulation of the experimental measurements, one would require a functional definition of the jet, for example using an angular cone, which will then define the jet energy E_{jet} , and hence x_K . The transverse momentum of the K^0 s, $p_T(K^0)$ (in GeV), is shown in the right hand frame in Fig 1. In both of these frames, the solid histograms correspond to the decay $t \rightarrow Ws$ and the dashed ones to the decay $t \rightarrow Wb$. As expected, the decay chain $t \rightarrow Ws(\rightarrow K_S^0)$ has a much stiffer distribution both in X_K and $p_T(K^0)$, as the K^0 's descending from the decay chain $t \rightarrow Wb(\rightarrow c \rightarrow s)$ are rapidly degraded in these variables due to the subsequent weak decays. The corresponding distributions for the Λ s are shown in the lower two frames in Fig. 1. They are qualitatively very similar to those of the K^0 s.

We now show the distributions in the charged lepton energy from the decays $t \rightarrow b \rightarrow \ell^\pm X$ and $t \rightarrow s \rightarrow \ell^\pm X$ in Fig. 2, showing the scaled lepton energy in the variable $X_\ell = E_\ell/E_{\text{jet}}$ (upper frame) and in p_T^ℓ , the transverse momentum of the charged leptons (middle frame). This distribution quantifies the richness of the b -jets in charged leptons and the stiff character of the energy/transverse momentum distributions due to the weak decays, as compared to the leptons

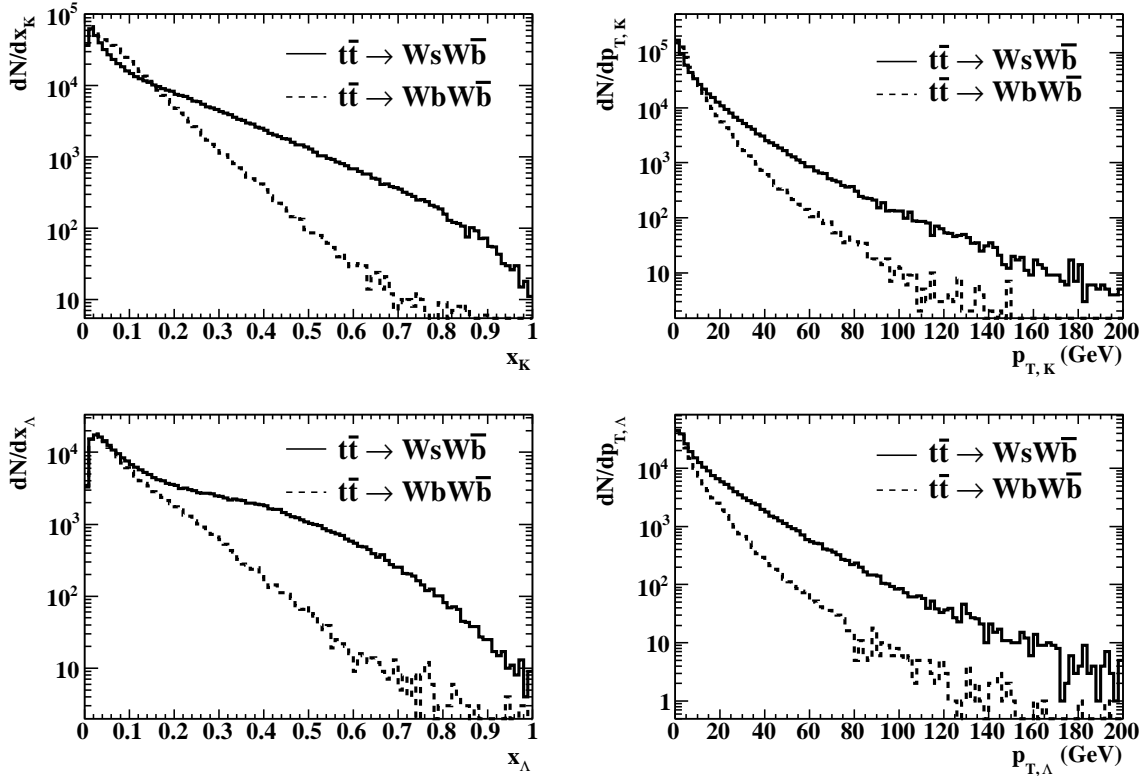


FIG. 1: $pp \rightarrow t\bar{t}X$ at $\sqrt{s} = 14$ TeV. Upper left frame: scaled- K^0 -energy distributions dN/dx_K from $t \rightarrow W s(\rightarrow K^0X)$ (solid histogram) and $t \rightarrow W b(\rightarrow K^0X)$ (dashed histogram). Upper right frame: Transverse momentum distributions of the K^0 s measured w.r.t. beam axis $dN/dp_{T,K}$ (in GeV) in the same production and decay processes as in the left frame. Lower frames show the distributions dN/dx_Λ and $dN/dp_{T,\Lambda}$ (in GeV) for $t \rightarrow W s(\rightarrow \Lambda X)$ (solid histogram) and $t \rightarrow W b(\rightarrow \Lambda X)$ (dashed histogram).

from $s \rightarrow \ell^\pm X$, which are all soft and coming from the leptonic decays of the various resonances produced in the fragmentation of the s -quark. Absence of energetic charged leptons in the s -quark jet in the decay $t \rightarrow W s$ is a powerful tool in reducing the background from the otherwise much more prolific process $t \rightarrow W b$. The final set of distributions from our Monte Carlo simulation is the secondary decay vertex distribution (lower frame), smeared with a Gaussian distribution with a r.m.s. of 2 millimetres, shown in terms of a variable called r (measured in millimetres). The decay length for the $t \rightarrow W b$ case is calculated as $\gamma c\tau_b$, where γ is the Lorentz factor, and $c\tau_b = 0.45$ mm, corresponding to an average b -quark lifetime taken as $\tau_b = 1.5$ ps from the PDG [14]. This distribution, which reflects the long lifetime of the b -quark (respectively of the B and Λ_b hadrons), as opposed to the lack of a secondary vertex from the s -quark fragmentation process, is also a very powerful discriminant of $t \rightarrow W b$ vs. $t \rightarrow W s$ decays.

Having generated these distributions, characterising the signal $t \rightarrow W s$ and background $t \rightarrow W b$ events in the process $pp \rightarrow t\bar{t}X$ at the LHC, we use the BDT and BDTD classifiers, discussed

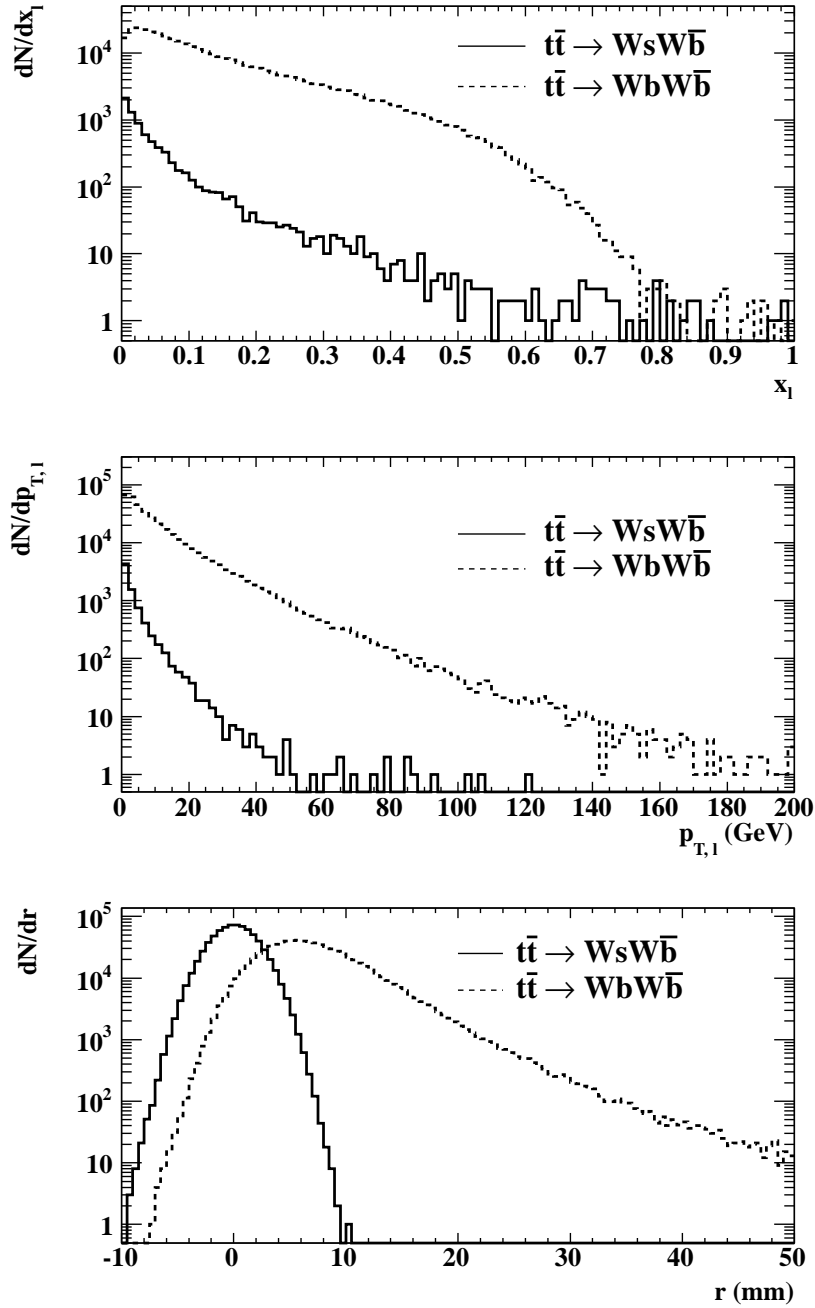


FIG. 2: $pp \rightarrow t\bar{t}X$ at $\sqrt{s} = 14$ TeV. Upper frame: scaled- ℓ^\pm -energy distributions, dN/dx_ℓ , from $t \rightarrow Ws$ ($\rightarrow \ell^\pm X$) (solid histogram) and $t \rightarrow Wb$ ($\rightarrow \ell^\pm X$) (dashed histogram). Middle frame: Transverse momentum distributions of the ℓ^\pm s measured w.r.t. beam axis, $dN/dp_{T,\ell}$ (in GeV), in the same production and decay processes as in the upper frame. Lower frame: Secondary decay vertex distributions in the variable r (in millimetres) for the two decay chains $t \rightarrow Ws$ (solid histogram) and $t \rightarrow Wb$ (dashed histogram), obtained by smearing the decay length with a Gaussian having an r.m.s. value of 2 mm.

in the introduction. In Fig. 3 (left frame), we show the BDTD response functions, showing that a clear separation between the signal ($t \rightarrow W s$) and background ($t \rightarrow W b$) events has been achieved. The background rejection vs. signal efficiency for the $pp \rightarrow t\bar{t}$ events is shown in Fig. 3 (right frame) for both the BDT and BDTD classifiers, which give very similar results. The evaluation results ranked by the best signal efficiency and purity are shown numerically in Table 1. The entries in this table show that a background rejection of 10^3 can be achieved at a signal efficiency of about 5% to reach the SM-sensitivity of the CKM matrix element $|V_{ts}|$. The statistical uncertainty in this efficiency is 0.026%. It goes up to 0.067% for efficiency values at the upper end.

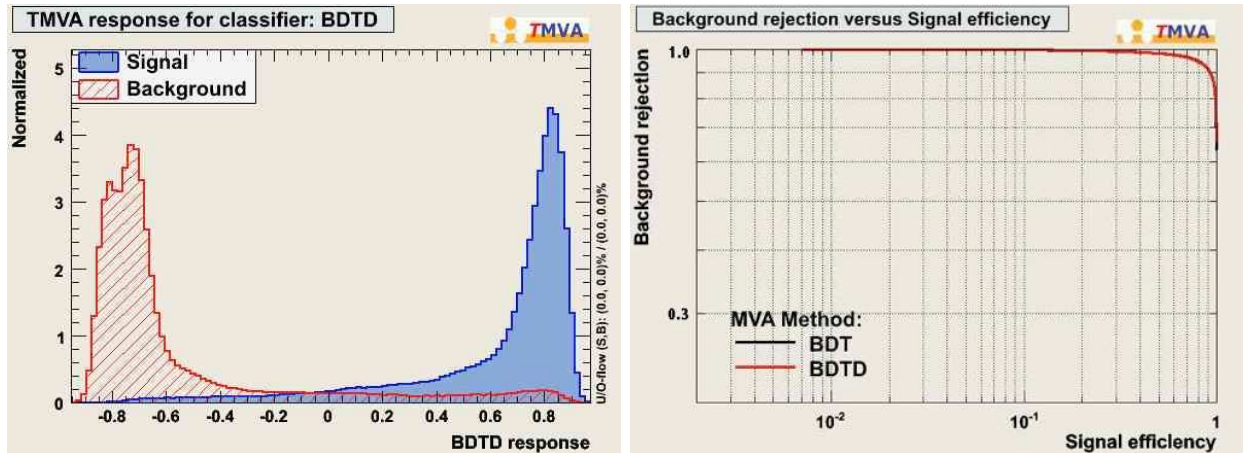


FIG. 3: $pp \rightarrow t\bar{t}X$ at $\sqrt{s} = 14$ TeV. Left frame: The normalised BDTD response, calculated by using the TMVA (see text). The signal (dark shaded) from the decay $t \rightarrow W s$ and the background (light shaded with dotted lines) from the decay $t \rightarrow W b$ are clearly separated in this variable. Right frame: Background rejection vs. signal efficiency calculated from the BDT(D) response. The result using the BDT classifier is very similar and hardly distinguishable from the one obtained with the BDTD response.

The distributions at $\sqrt{s} = 7$ and 10 TeV are very similar to the corresponding ones shown in Fig. 1 for 14 TeV. Hence, the characteristic differences that we have shown at $\sqrt{s} = 14$ TeV emanating from the top quark decays $t \rightarrow Wb$ and $t \rightarrow Ws$ in the $V0$ and charged lepton energy- and transverse momentum spectra are also present at the lower energies.

Based on the above analysis we have calculated the tagging efficiencies for the decay $t \rightarrow W s$ (signal) for an acceptance of 0.1% for the decay $t \rightarrow Wb$ (background). The acceptance level is motivated by the anticipated value of the ratio of the $t \rightarrow Ws$ and $t \rightarrow Wb$ decay rates, which in the SM is $O(10^{-3})$. The tagging efficiencies for the three centre-of-mass energies at the LHC (7, 10 and 14 TeV) are given in Table 1 for two different vertex smearing (1 mm and 2 mm), assuming a Gaussian distribution. The entries shown as bb/bs correspond to the comparison for top pair production process $pp \rightarrow t\bar{t}X$ with both the t and \bar{t} decaying via the dominant process $t \rightarrow W^+b$ and $\bar{t} \rightarrow W^-b$, respectively, and in which only one of the t or \bar{t} quarks decays via $t \rightarrow W^+s$ or

TABLE I: Tagging efficiencies (in %) for the process $pp \rightarrow t\bar{t}X$, followed by the decay $t \rightarrow Ws$ (signal) and $t \rightarrow Wb$ (background), calculated for an acceptance of 0.1% for the background at three LHC centre-of-mass energies. Two Gaussian vertex smearing (having an r.m.s. values of 2 mm and 1 mm) are assumed for calculating the displaced vertex distributions dN/dr . The cases bb/bs and bs/ss are explained in the text.

bb/bs	vertex smearing	7 TeV	10 TeV	14 TeV
	2 mm	5.1	5.6	5.0
	1 mm	20.5	15.4	15.5
bs/ss	vertex smearing	7 TeV	10 TeV	14 TeV
	2 mm	13.2	9.6	12.3
	1 mm	30.6	24.2	34.2

$\bar{t} \rightarrow W^- \bar{s}$, and the other decays via $t \rightarrow W^+ b$ or $\bar{t} \rightarrow W^- \bar{b}$ (signal events). The entries marked as bs/ss correspond to the cases where either the t or \bar{t} quarks decays via $t \rightarrow W^+ s$ or $\bar{t} \rightarrow W^- \bar{s}$ and both t and \bar{t} quarks decay via $t \rightarrow W^+ s$ and $\bar{t} \rightarrow W^- \bar{s}$. The branching ratio for the case $(t \rightarrow W^+ s)(\bar{t} \rightarrow W^- \bar{s})$ is exceedingly small, $O(10^{-6})$. The entries in Table 1 for this case (bs/ss) show that at the considerable price of the reduced sample, one can get much better efficiencies.

III. ANALYSIS OF THE PROCESS $pp \rightarrow t/\bar{t}X$ AND THE SUBSEQUENT DECAYS $t \rightarrow Wb, Ws$

The single top (or anti-top) cross sections in hadron hadron collisions have been calculated in the NLO approximation [9, 10, 30–32]. Recalling that there are three basic processes at the leading order which contribute to $\sigma(pp \rightarrow t/\bar{t}X)$, namely the t -channel: $qb \rightarrow q't$, the s -channel: $q\bar{q}' \rightarrow \bar{b}t$; and the associated tW production $bg \rightarrow tW^-$, the cross sections estimated at the Tevatron are [29]: $\sigma^{t\text{-channel}}(pp \rightarrow tX) = \sigma(pp \rightarrow \bar{t}X) = 1.14 \pm 0.06$ pb, $\sigma^{s\text{-channel}}(pp \rightarrow tX) = \sigma(pp \rightarrow \bar{t}X) = 0.53 \pm 0.02$ pb, and $\sigma^{tW\text{-channel}}(pp \rightarrow tX) = \sigma(pp \rightarrow \bar{t}X) = 0.14 \pm 0.03$ pb, putting the single top (or antitop) cross section $\sigma(pp \rightarrow tX) = \sigma(pp \rightarrow \bar{t}X) \simeq 1.8$ pb at the Tevatron. These cross sections have to be compared with the theoretically projected cross sections at the LHC@14 TeV: $\sigma^{t\text{-channel}}(pp \rightarrow tX) = 149 \pm 6$ pb, $\sigma^{t\text{-channel}}(pp \rightarrow \bar{t}X) = 91 \pm 4$ pb, $\sigma^{s\text{-channel}}(pp \rightarrow tX) = 7.7^{+0.6}_{-0.7}$ pb, $\sigma^{s\text{-channel}}(pp \rightarrow \bar{t}X) = 4.3 \pm 0.2$ pb, and $\sigma^{tW\text{-channel}}(pp \rightarrow tX) = \sigma(pp \rightarrow \bar{t}X) = 43 \pm 5$ pb. Thus, one expects $\sigma(pp \rightarrow tX) \simeq 200$ pb and about half this number for $\sigma(pp \rightarrow \bar{t}X)$, yielding the summed single top and antitop cross sections at about 300 pb at the LHC@14 TeV, also approximately two orders of magnitude larger than those at the Tevatron. With a luminosity of 10 fb^{-1} , one anticipates $O(3 \times 10^6)$ single top (or anti-top) events, i.e. $O(10^6)$ events in the leptonic

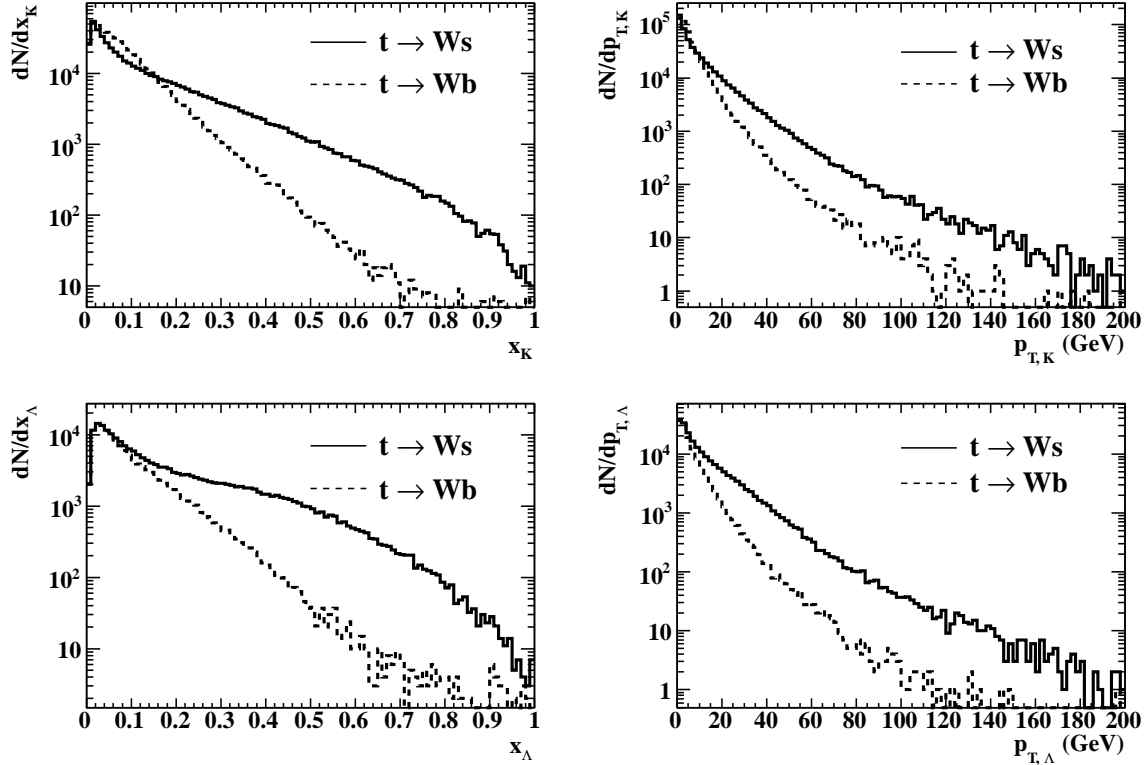


FIG. 4: $pp \rightarrow t/\bar{t}X$ at $\sqrt{s} = 14$ TeV. Upper frames: Scaled energy distributions dN/dx_K and the transverse momentum distribution $dN/dp_{T,K}$ from the decays $t \rightarrow Ws(\rightarrow K^0 X)$ (solid histograms) and $t \rightarrow Wb(\rightarrow K^0 X)$ (dashed histograms). Lower frames: Scaled energy distributions dN/dx_Λ and the transverse momentum distribution $dN/dp_{T,\Lambda}$ from the decays $t \rightarrow Ws(\rightarrow \Lambda X)$ (solid histograms) and $t \rightarrow Wb(\rightarrow \Lambda X)$ (dashed histograms).

channel. Thus, the rise in the cross sections for a single top (or antitop) production between the Tevatron and the LHC@14 TeV is also very marked.

In the analysis shown here, we have again resorted to the Monte Carlo generator PYTHIA, which models so far only the s -channel single top production process $pp \rightarrow W \rightarrow t\bar{b}$. As discussed above, this has the smallest (of the three channel) cross section. Moreover, the tW channel process $bg \rightarrow tW^-$ provides a much more efficient trigger in terms of the W^- accompanying the top quark. So, the analysis presented in this section should be repeated with a more complete code, including all three channels. However, we think that in estimating the various efficiencies, the current version of PYTHIA is adequate. The distributions in the scaled energy variable X_K and in the transverse momentum p_T of the K^0 s produced in the process $pp \rightarrow t/\bar{t}X$, and the subsequent decays $t \rightarrow Ws$ and $t \rightarrow Wb$ are shown in Fig. 4 (upper two frames) for $\sqrt{s} = 14$ TeV. The corresponding distributions for the Λ s from the decays $t \rightarrow Ws(\rightarrow \Lambda X)$ and $t \rightarrow Wb(\rightarrow \Lambda X)$ are shown in the lower two frames in Fig 4. The scaled charged lepton energy distribution $X_\ell = E_\ell/E_{\text{jet}}$ and the

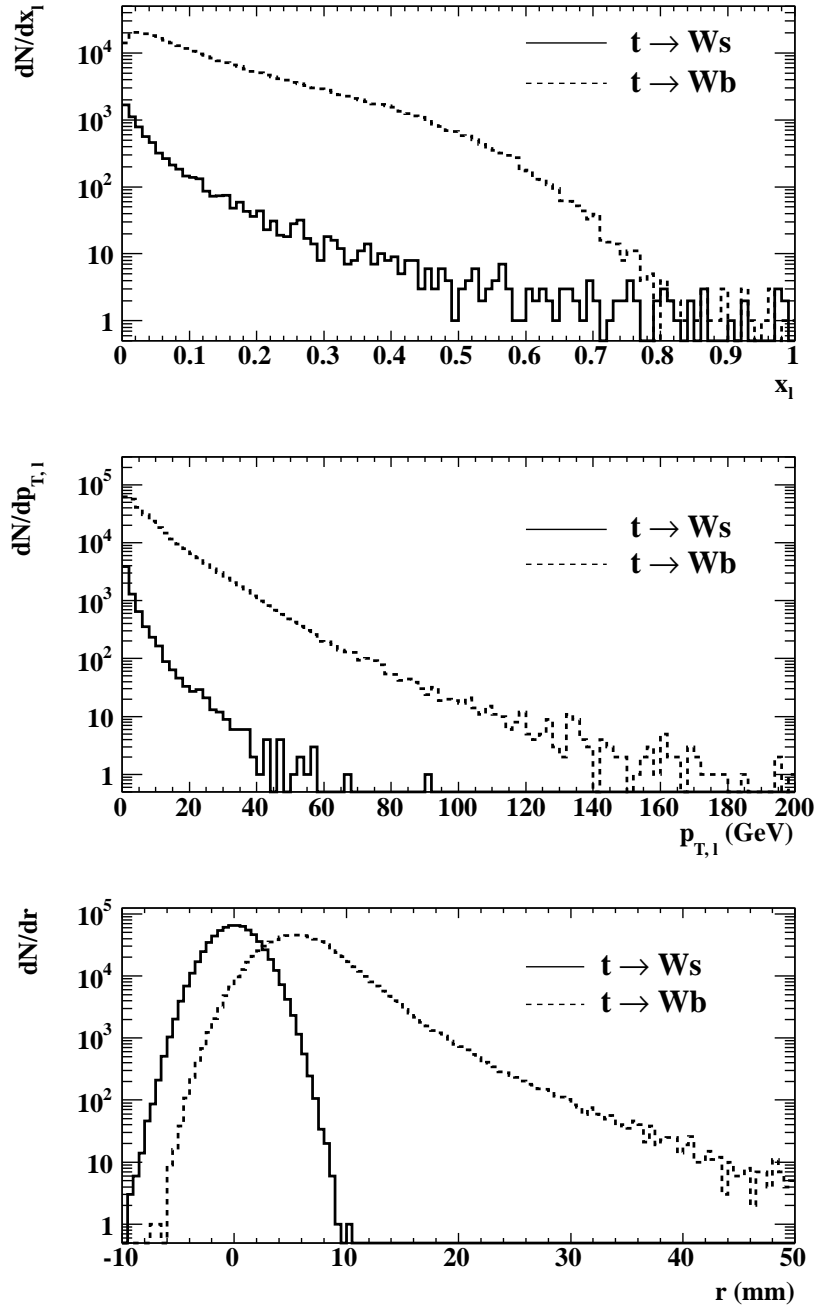


FIG. 5: $pp \rightarrow t/\bar{t}X$ at $\sqrt{s} = 14$ TeV. Upper frame: scaled- ℓ^\pm -energy distributions, dN/dx_ℓ , from $t \rightarrow Ws$ ($\rightarrow \ell^\pm X$) (dashed histogram) and $t \rightarrow Wb$ ($\rightarrow \ell^\pm X$) (solid histogram). Middle frame: Transverse momentum distributions of the ℓ^\pm s measured w.r.t. beam axis, $dN/dp_{T,\ell}$ (in GeV), in the same production and decay processes as in the upper frame. Lower frame: Secondary decay vertex distributions in the variable r (in millimetres) for the two decay chains $t \rightarrow Ws$ (solid histogram) and $t \rightarrow Wb$ (dashed histogram), obtained by smearing the decay length with a Gaussian having an r.m.s. value 2 millimetres.

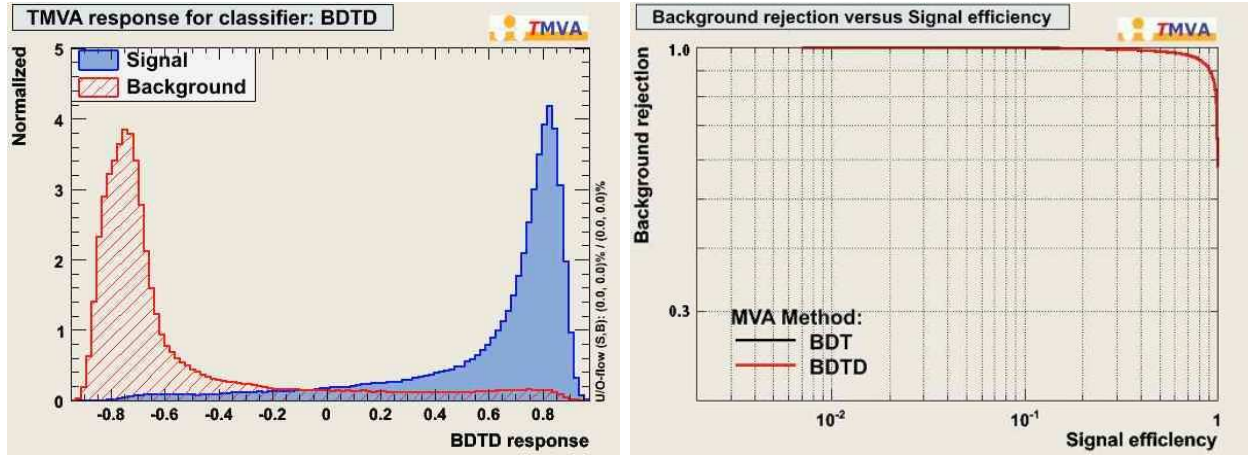


FIG. 6: $pp \rightarrow t/\bar{t}X$ at $\sqrt{s} = 14$ TeV. Left: The normalised BDTD response, calculated by using the TMVA (see text). The signal (dark shaded) from the decay $t \rightarrow Ws$ and the background (light shaded with dotted lines) from the decay $t \rightarrow Wb$ are clearly separated in this variable. Right: Background rejection vs. signal efficiency calculated from the BDT(D) response. The two MVA methods yield very similar results.

lepton transverse momentum are shown in Fig. 5 (upper frame), showing the distributions from the $t \rightarrow Wb(\rightarrow \ell^\pm X)$ (dashed histograms) and $t \rightarrow Ws(\rightarrow \ell^\pm X)$ (solid histograms). Transverse momentum distributions of the ℓ^\pm s, measured w.r.t. the axis, are also shown in this figure (middle frame). Finally, the secondary decay vertex distribution for the decays $t \rightarrow Wb$ (dashed histogram) and $t \rightarrow Ws$ (solid histogram) are shown in the lower frame in this figure. In plotting these distributions, we have smeared them, as before, with a Gaussian with a r.m.s. value of 2 millimetres and have taken into account the finite lifetime of the b -quark, as stated in the case of the analysis for the process $pp \rightarrow t\bar{t}X$. These distributions provide an excellent discrimination between the signal $t \rightarrow Ws$ and the dominant background $t \rightarrow Wb$ events for the single top production process $pp \rightarrow t/\bar{t}X$, qualitatively very much along the same lines as discussed earlier for the $t\bar{t}$ production $pp \rightarrow t\bar{t}X$. As already stated, this information is used to build up a decision tree. In Fig. 6 (left frame), we show that the BDTD response function is very different for the signal ($t \rightarrow Ws$) and the background ($t \rightarrow Wb$) events also for the single top (antitop) production process. The background rejection vs. signal efficiency for the $pp \rightarrow t/\bar{t}X$ events is shown in Fig. 6 (right frame). The results for the signal efficiency and purity are shown numerically in Table II. The entries in this table show that also in single top production process a background rejection of 10^3 can be achieved at a signal efficiency of about 5% to 7% to reach the SM-sensitivity of the CKM matrix element $|V_{ts}|$. Thus we would expect $0.053 \times 1.7 \times 10^{-3} \times 10^6 = 90$ signal events with a background of $10^{-3} \times 10^6 = 10^3$ events giving a significance of $90/\sqrt{1000}$ i.e. about 3σ .

TABLE II: Tagging efficiencies (in %) for the single top production process $pp \rightarrow t/\bar{t}X$, followed by the decay $t \rightarrow Ws$ (signal) and $t \rightarrow Wb$ (background), calculated for an acceptance of 0.1% for the background at three LHC centre-of-mass energies. Two Gaussian vertex smearing (having an r.m.s. values 2 mm and 1 mm) are assumed for calculating the displaced vertex distributions dN/dr .

σ_0	7 TeV	10 TeV	14 TeV
2 mm	7.1	6.5	5.3
1 mm	21.7	22.4	19.9

IV. SUMMARY AND OUTLOOK

We have presented a case here to measure the matrix element $|V_{ts}|$ from the top quark decays $t \rightarrow W^+s$ and its charge conjugate $\bar{t} \rightarrow W^-\bar{s}$, making use of the characteristic differences in the b - and s -jet profiles. We have concentrated on the V0 (K^0 and Λ) energy-momentum profiles emanating from the signal ($t \rightarrow Ws$) and the dominant background ($t \rightarrow bW$). This information is combined with the secondary vertex distributions, anticipated from the decays ($b \rightarrow c \rightarrow s$), and the absence of energetic charged leptons in s -quark jets. An important parameter is the vertex resolution, for which we have used two values, $\sigma(\text{vertex}) = 1$ mm and 2 mm, assuming a Gaussian distribution. With these distributions, we train boosted decision tree classifiers, BDT and BDTD, and use the BDT(D)-response functions for the signal ($t \rightarrow Ws$) and background ($t \rightarrow bW$) events. This information is used to study the background rejection versus the signal efficiency, which would enable to achieve typically 10% signal efficiency and a background rejection of 10^3 . Detailed studies are done at three representative values of the LHC centre-of-mass energies, $\sqrt{s} = 7$ TeV, 10 TeV and 14 TeV. As the principal results (BDT(D) response functions and background rejection versus signal efficiencies) are very similar for all three energies, we present detailed results only for $\sqrt{s} = 14$ TeV.

In this exploratory study, we have made some simplifying assumptions. In particular, we have used PYTHIA to undertake our analysis. The cross sections for the top pair ($pp \rightarrow t\bar{t}X$) and single top production ($pp \rightarrow t/\bar{t}X$) in PYTHIA can be adjusted to correspond to the theoretical precision currently available. However, the distributions and topologies, in particular for the single top (anti-top) production processes, will have to be correctly incorporated in a realistic simulation. Likewise, we have not attempted to define the s - and b -quark jets using a modern jet algorithm. No attempt has been made at improving the training process by adding some more variables, like the b -jet shapes [36], which are known to have some discriminating power. We recall some of the important sources of uncertainties in our analysis: (i) predicted rates of the top quark production,

(ii) histogram shapes, (iii) integrated luminosities, (iv), efficiencies of the b - and s -quark tagging, reflecting in our study the relative efficiencies given in Tables I and II, and the uncertainty in m_t , though this effect mainly the CKM matrix element determinations form the single top (anti-top) production processes. All these experimental and theoretical refinements will have to be incorporated in the analysis of the LHC data to draw quantitative conclusions. In particular, background processes, most notably $W + jets$, $Z + jets$ will have to be considered. Nevertheless, we have shown, in the first study of its kind, that a *direct measurement* of $|V_{ts}|$ in top quark decays is, in principle, feasible at the LHC. The simulations presented here for 14 TeV correspond to an integrated luminosity of 10 fb^{-1} .

Alternative methods of determining the matrix elements $|V_{td}|$, $|V_{ts}|$ and $|V_{tb}|$ at the LHC are based on the single top (or anti-top) production at the LHC. One attempts to determine these matrix elements from the cross section measurement by a simultaneous fit. This cross section is parametrised as $\sigma(pp \rightarrow tX) = A_d|V_{td}|^2 + A_s|V_{ts}|^2 + A_b|V_{tb}|^2$ (and likewise for $\sigma(pp \rightarrow \bar{t}X)$), one then solves the cross-section for the CKM matrix elements, given the dynamical quantities A_d , A_s and A_b . They, in turn, depend on estimates of the various electroweak processes in the single-top (or anti-top) production and on the parton distribution functions (PDFs). Typical estimates of the reduced cross sections at the LHC ($\sqrt{s} = 14 \text{ TeV}$) are: $A_d = 766(253) \text{ pb}$, $A_s = 277(172) \text{ pb}$, and $A_t = 150(87) \text{ pb}$ [37], where the numbers in the parenthesis refer to the production of anti-top at the LHC. Based on these estimates, one expects at the LHC $A_s/A_b \sim 2$ and $A_d/A_b \sim 5$. These ratios depend on QCD and hence will not change if the weak interactions in the SM are modified by new physics. In the SM, one expects $|V_{ts}|^2/|V_{tb}|^2 \sim 1.6 \times 10^{-3}$ and $|V_{td}|^2/|V_{tb}|^2 \sim 6 \times 10^{-5}$. In the example of realistic beyond-the SM physics that we are using to motivate these studies, these CKM matrix element ratios could be larger by a factor 4. We conclude that both in the SM, and in the four generation extension of it, the cross sections $\sigma(pp \rightarrow tX)$ and $\sigma(pp \rightarrow \bar{t}X)$ are completely dominated by the $A_b|V_{tb}|^2$ term. Hence, this proposal does not have the desired sensitivity to measure the matrix elements $|V_{td}|$ and $|V_{ts}|$ at the level of theoretical interest,

It has been recently suggested in [38] that one may improve the sensitivity to $|V_{td}|$, if one refines the experimental analysis using the top quark rapidity distributions, which are different for the valence d -quark initiated processes as opposed to the sea b -quark initiated processes [38]. While of some value in exploring $|V_{td}|$, still the sensitivity of this method is far from the expected value of $|V_{td}|$ by an order of magnitude. Moreover, as the s -quark and the b -quark are both sea-quarks in the proton, the top quark rapidity distributions do not provide an improved determination of $|V_{ts}|$ from the single top production process. Hence, our method based on the top quark decay characteristics to determine $|V_{ts}|$ complements the existing proposal.

Finally, we remark that the ratio of the CKM matrix elements $(|V_{td}|^2 + |V_{ts}|^2)/|V_{tb}|^2$, that can

be obtained by measuring the ratio R_t , defined in the introduction, through the number of events with zero-, one-, and two b -tags in the process $pp \rightarrow t\bar{t}X$, can be combined with the determination of the ratio $|V_{ts}|^2/|V_{tb}|^2$ discussed here, to constrain (or measure) the quantity $|V_{td}|^2/|V_{tb}|^2$.

Acknowledgements: We thank Karl Jakobs and Torbjorn Sjostrand for helpful discussions. Helpful communication with Alexander Lenz is also thankfully acknowledged.

-
- [1] F. Abe *et al.* [CDF Collaboration], Phys. Rev. Lett. **74**, 2626 (1995) [arXiv:hep-ex/9503002].
 - [2] S. Abachi *et al.* [D0 Collaboration], Phys. Rev. Lett. **74**, 2632 (1995) [arXiv:hep-ex/9503003].
 - [3] [Tevatron Electroweak Working Group and CDF Collaboration and D0 Collab], arXiv:0903.2503 [hep-ex].
 - [4] V. M. Abazov *et al.* [D0 Collaboration], Phys. Rev. Lett. **103**, 092001 (2009) [arXiv:0903.0850 [hep-ex]].
 - [5] T. Aaltonen *et al.* [CDF Collaboration], Phys. Rev. Lett. **103**, 092002 (2009) [arXiv:0903.0885 [hep-ex]].
 - [6] N. Cabibbo, Phys. Rev. Lett. **10**, 531 (1963).
 - [7] M. Kobayashi and T. Maskawa, Prog. Theor. Phys. **49**, 652 (1973).
 - [8] L. Wolfenstein, Phys. Rev. Lett. **51**, 1945 (1983).
 - [9] N. Kidonakis, Phys. Rev. D **74**, 114012 (2006) [arXiv:hep-ph/0609287].
 - [10] B. W. Harris, E. Laenen, L. Phaf, Z. Sullivan and S. Weinzierl, Phys. Rev. D **66**, 054024 (2002) [arXiv:hep-ph/0207055].
 - [11] T. E. W. Group [CDF Collaboration and D0 Collaboration], arXiv:0908.2171 [hep-ex].
 - [12] D. E. Acosta *et al.* [CDF Collaboration], Phys. Rev. Lett. **95**, 102002 (2005) [arXiv:hep-ex/0505091].
 - [13] V. M. Abazov *et al.* [D0 Collaboration], Phys. Rev. Lett. **100**, 192003 (2008) [arXiv:0801.1326 [hep-ex]].
 - [14] C. Amsler *et al.* [Particle Data Group], Phys. Lett. B **667**, 1 (2008).
 - [15] O. Eberhardt, A. Lenz and J. Rohrwild, arXiv:1005.3505 [hep-ph].
 - [16] J. Han and M. Kamber, Data mining concepts and techniques, Elsevier 2006.
 - [17] Z. Liu, FERMILAB-THESIS-2009-45.
 - [18] A. Hocker *et al.*, PoS A **CAT**, 040 (2007) [arXiv:physics/0703039].
 - [19] T. Sjostrand, S. Mrenna and P. Z. Skands, Comput. Phys. Commun. **178**, 852 (2008) [arXiv:0710.3820 [hep-ph]].
 - [20] “Expected performance of the ATLAS experiment: Detector, Trigger and Physics”, G. Aad *et al.* [ATLAS Collaboration], arXiv:0901.0512 (2009); “The ATLAS experiment at the Large Hadron Collider”, G. Aad *et al.* [ATLAS Collaboration], JINST 3: S08003 (2008).
 - [21] “The CMS experiment at the CERN Large Hadron Collider”, R. Adolphi *et al.* [CMS Collaboration], JINST 3: S08004 (2008).
 - [22] R. Bonciani, S. Catani, M. L. Mangano and P. Nason, Nucl. Phys. B **529**, 424 (1998) [Erratum-ibid. B **803**, 234 (2008)] [arXiv:hep-ph/9801375].
 - [23] M. Cacciari, S. Frixione, M. L. Mangano, P. Nason and G. Ridolfi, JHEP **0809**, 127 (2008) [arXiv:0804.2800 [hep-ph]].

- [24] N. Kidonakis and R. Vogt, Phys. Rev. D **78**, 074005 (2008) [arXiv:0805.3844 [hep-ph]].
- [25] S. Moch and P. Uwer, Phys. Rev. D **78**, 034003 (2008) [arXiv:0804.1476 [hep-ph]].
- [26] A. D. Martin, W. J. Stirling, R. S. Thorne and G. Watt, Phys. Lett. B **652**, 292 (2007) [arXiv:0706.0459 [hep-ph]].
- [27] P. M. Nadolsky *et al.*, Phys. Rev. D **78**, 013004 (2008) [arXiv:0802.0007 [hep-ph]].
- [28] U. Langenfeld, S. Moch and P. Uwer, arXiv:0907.2527 [hep-ph].
- [29] N. Kidonakis, Nucl. Phys. A **827**, 448C (2009) [arXiv:0901.2155 [hep-ph]].
- [30] Q. H. Cao, R. Schwienhorst and C. P. Yuan, Phys. Rev. D **71**, 054023 (2005) [arXiv:hep-ph/0409040].
- [31] S. Heim, Q. H. Cao, R. Schwienhorst and C. P. Yuan, Phys. Rev. D **81**, 034005 (2010) [arXiv:0911.0620 [hep-ph]].
- [32] N. Kidonakis, Phys. Rev. D **75**, 071501 (2007) [arXiv:hep-ph/0701080].
- [33] N. Kidonakis, Acta Phys. Polon. B **39**, 1593 (2008) [arXiv:0802.3381 [hep-ph]].
- [34] N. Kidonakis, arXiv:1001.5034 [hep-ph].
- [35] N. Kidonakis and G. Sterman, Phys. Lett. B **387** (1996) 867; N. Kidonakis and G. Sterman, Nucl. Phys. B **505**, 321 (1997) [arXiv:hep-ph/9705234].
- [36] T. Aaltonen *et al.* [CDF Collaboration], Phys. Rev. D **78**, 072005 (2008) [arXiv:0806.1699 [hep-ex]].
- [37] J. Alwall *et al.*, Eur. Phys. J. C **49**, 791 (2007) [arXiv:hep-ph/0607115].
- [38] J. A. Aguilar-Saavedra and A. Onofre, arXiv:1002.4718 [hep-ph].